DIMENSIONALITY REDUCTION TECHNIQUES WITH HYDRANET FRAMEWORK FOR HSI CLASSIFICATION

Mohammed Q. Alkhatib [1*], *Mina Al-Saad* [1], *Nour Aburaed* [1], *Saeed Al Mansoori* [2], *and Hussain Al Ahmad* [1]

[1] University of Dubai, College of Engineering and IT, Dubai,UAE
[2] Mohammed Bin Rashed Space Centre, Dubai, UAE
[*] mqalkhatib@ieee.org

ABSTRACT

Hyperspectral Imagery (HSI) classification is an important research area in remote sensing community due to its high efficiency in accurately analyzing ground features by assigning a class label to each pixel. This paper explores the use of Band Subset selection (BSS) methods as Dimensionality Reduction (DR) pre-processing stage for HSI classification, and compares them to Principal Component Analysis (PCA) approach. BSS is the problem of selecting the most independent bands in HSI cube. Classification is then performed using a proposed multi-branch HydraNet model that combines 1D, 2D, and 3D convolution. HydraNet is trained and tested using the benchmark Pavia University dataset, and the results are evaluated using Kappa and Overall Accuracy. Experimental results show positive indications of the network's performance, especially when compared to other state-of-the-art CNN networks.

Index Terms— HSI classification, Dimensionality reduction, Band Subset Selection, HydraNet.

1. INTRODUCTION

Hyperspectral Imagery (HSI) became a hot research area in the field of remote sensing. HSI can obtain spectral and spatial information simultaneously by providing hundreds of narrow contiguous spectral bands, ranging from visible to infrared wavelengths [1]. Nowadays, HSI has been widely employed in numerous remote sensing applications, such as environmental monitoring [2], military and security applications [3], and others. Among these applications, classification has attracted increasing attention in HSI data analysis. HSI classification is the task of assigning categories to every pixel in the image based on spectral characteristics and spatial context of each pixel. Unlike conventional RGB images, HSI carry additional information about the material's chemical and physical properties since the interaction between the materials and light varies depending on its atomic and molecular structure, which makes HSI rich in spectral information that facilitates image classification tasks [4]. HSI contains hundreds of spectral bands and redundant information, which makes feature analysis more challenging and computationally expensive. Hence, this can affect the classification performance. Thus, many researches presented various Dimensionality Reduction (DR) methods to overcome the curse of dimensionality of HSI data while preserving the same spatial information. Mounika et al. [5] introduced Principal Components Analysis (PCA) to reduce the dimensionality of the HSI images by eliminating the noise in the dataset prior to the classification using Support Vector Machine (SVM). The researchers in [6] used mean shift clustering to combine the spatial and spectral information and then classified the HSI by using a pseudo supervised fusion technique. Band Subset Selection (BSS) [7] is a DR technique that keeps spectral insight for further image exploitation. BSS can be based on physical insight, optimizing an information content measure, class separability, or other criteria. In HSI analysis, it is common to unfold the data cube into a matrix with columns and rows representing individual bands and the spectral signatures of individual pixels, respectively. BSS is related to the selection of a subset of columns from the resulting matrix. In linear algebra, selecting the most linearly independent or most representative subset of columns of a matrix is known as Column Subset Selection (CSS).

Recently, deep learning, especially Deep Convolutional Neural Networks (DCNNs), became a powerful tool for classifying the HSI data due to their ability to automatically learn and extract deep nonlinear features from data without human intervention. DCNN approaches applied for HSI classification are mainly divided into two categories: spectral-based approach and spectral–spatial-based approach [8]. For example, the authors in [9] proposed one dimensional CNN (1D-CNN) approach for directly classifying HSI in the spectral domain. Other researchers introduced a two dimensional CNN (2D-CNN) architecture for HSI classification with employing one DR technique known as randomized PCA (R-PCA) to reduce the HSI data prior to model training [10]. Kanthi et al. [11] presented a three dimensional CNN (3D-CNN)-based HSI classification model to classify HSI, in which both spectral and spatial information are utilized to boost the classification performance. Since 1D, 2D, and 3D CNNs utilize data dif-

ferently, it is worth investigating the possibility of boosting the performance by combining the efforts of each network. This can be achieved with a HydraNet model, an ensemble learning technique [12], which has not been utilized for HSI classification thus far.

The main contributions of this work are as follows:

- to investigate the use of BSS as a pre-processing stage for HSI classification, and how BSS methods perform compared to PCA. This work extends the research presented in [13].
- to build, train, and test a HydraNet-based model for HSI classification that combines the advantages of multiple classifiers, namely: 1D-CNN, 2D-CNN, and 3D-CNN [14].

The remaining sections are organized as follows: Section 2 presents the background and mathematical framework, Section 3 explains the proposed methodology, Section 4 demonstrates and discusses the experiments and results, and Section 5 summarizes and concludes the paper.

2. BACKGROUND AND MATHEMATICAL FRAMEWORK

2.1. Band Subset Selection and Dimensionality Reduction

BSS has several interesting advantages compared to other DR techniques since it preserves the physical meaning of the spectral bands that can be used to (a) maximize human understanding, (b) combine spectral data with other data types, and (c) exploit physical modeling or simulation. In terms of the matrix representation of the hyperspectral image $\mathbf{X} \in R^{N \times n}$, BSS can be stated as the problem of selecting a permutation matrix $\mathbf{\Pi}$ in

$$\boldsymbol{X\Pi} = [\boldsymbol{X_1}|\boldsymbol{X_2}] \tag{1}$$

such that $\mathbf{X}_1 \in R^{N \times p}$, the matrix of "*selected bands*", has some particular properties of interest. $\mathbf{X}_2 \in R^{N \times (n-p)}$ is the matrix of "*redundant bands*". Here N is the number of pixels, and *n* is the number of spectral bands. Clearly, this formulation helps to relate BSS to CSS [15]. Further details on the mathematical formulation can be found in [16].

2.2. Column Subset Selection Algorithms

This section describes the CSS algorithms used in this paper for unsupervised BSS, namely Singular Values Decomposition Subset Selection (SVDSS), and Rank Revealing QR (RRQR) Factorization.

2.2.1. SVDSS

This algorithm for CSS was proposed in [17]. Let $\boldsymbol{X} = \boldsymbol{U\Sigma V^T}$ be the SVD for $\mathbf{X}$. Note that

$$\mathbf{X\Pi} = [\mathbf{X_1}|\mathbf{X_2}] = \mathbf{U\Sigma V^T\Pi} \tag{2}$$

Therefore, permuting the columns of $\mathbf{X}$ is equivalent to permuting the rows of $\mathbf{V}$. Moreover, selecting a particular column from $\mathbf{X}$ amounts to selecting the corresponding row in $\mathbf{V}$. Let

$$\bar{\mathbf{V}} = \mathbf{\Pi^T V} = \begin{bmatrix} \bar{\mathbf{V}}_{11} & \bar{\mathbf{V}}_{12} \\ \bar{\mathbf{V}}_{21} & \bar{\mathbf{V}}_{22} \end{bmatrix}$$

be a partitioning of the row-wise permuted matrix of right singular vectors commensurate with the partitioning in (1). It is shown in [15, 17] that a good $\mathbf{\Pi}$ is one that results in $||\bar{\mathbf{V}}_{11}^{-1}|| \approx 1$, which can be obtained from the QR factorization with pivoting [15, 17] on the matrix $\mathbf{V}_1^T$ corresponding to the first *p* right singular vectors of $\mathbf{X}$.

2.2.2. RRQR Factorization

The QR factorization can also be used for CSS [18]. The QR factorization of $\mathbf{X}$ with column pivoting is given by

$$\mathbf{X\Pi} = [\mathbf{X_1}|\mathbf{X_2}] = \mathbf{QR} = [\mathbf{Q_1}\ \mathbf{Q_2}] \begin{bmatrix} \mathbf{R}_{11} & \mathbf{R}_{12} \\ \mathbf{0} & \mathbf{R}_{22} \end{bmatrix} \tag{3}$$

A couple of important observations are that $\mathbf{X}$ and $\mathbf{R}$ have the same singular values, and that

$$\mathbf{X}_1 = \mathbf{Q}_1\mathbf{R}_{11}, \mathbf{X}_2 = [\mathbf{Q}_1\ \mathbf{Q}_2] \begin{bmatrix} \mathbf{R}_{12} \\ \mathbf{R}_{22} \end{bmatrix}$$

Furthermore,

$$||\mathbf{X}_2 - \mathbf{X}_1\mathbf{X}_1^{\#}\mathbf{X}_2||_F^2 = ||\mathbf{R}_{21}||_F^2$$

where $\mathbf{X}^{\#}$ is the pseudo-inverse of $\mathbf{X}$. This specific type of QR factorization is called the RRQR factorization [19].

3. METHODOLOGY AND NETWORK ARCHITECTURE

HydraNet consists of a multi-branch DCNN that was originally devised by [12] in 2018. Ever since then, this model has been utilized in various different image processing tasks, such as image classification and de-noising. However, this model has not been utilized for HSI classification thus far. Therefore, a HydraNet model framework is proposed for HSI classification. One of the main advantages HydraNet provides is feature sharing. It has been established in the literature that 1D-, 2D-, and 3D-CNNs have different advantages for HSI classification. If these advantages can be combined while reducing repetitive calculations, the final outcome produced by HydraNet can outperform its individual components. Our methodology uses three state-of-the-art CNN architectures published in [14]; 1D-CNN, 2D-CNN, and 3D-CNN. The architecture of the proposed model is as shown in Fig.1

This network is integrated with three different DR techniques, namely PCA, SVDSS, and RQRR, as pre-processing steps, such that their effect on the overall HydraNet performance can be studied.

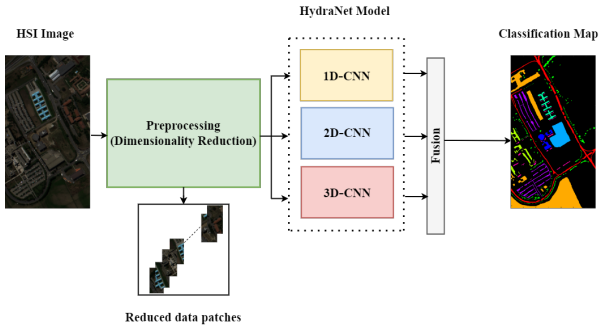

Fig. 1: Flowchart of the proposed HydraNet model for HSI classification.

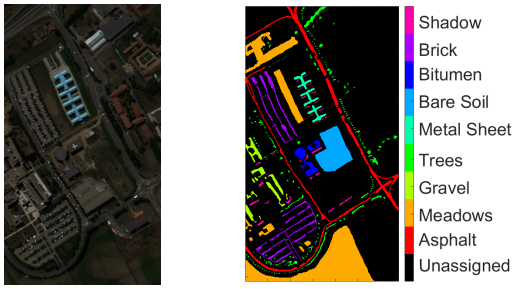

(a) (b)

Fig. 2: (a) True color RGB image of Pavia University and (b) Classification map

4. EXPERIMENTS AND ANALYSIS

4.1. Hyperspectral Data and Implementation Details

To demonstrate the performance of proposed network, we evaluate it on the Pavia University scene. This scene is acquired with the ROSIS sensor during a flight campaign over Pavia, northern Italy. The dataset consists of 103 spectral bands in the wavelength range from 430 to 860 nm with a spatial resolution of 1.3m and 610×340 pixels per band. The classification map contains nine classes: Asphalt, Meadows, Gravel, Trees, Metal Sheet, Bare Soil, Bitumen, Brick and Shadow. The unassigned pixels in the image are colored in black [20]. The RGB image and classification map for the Pavia University scene are shown in Figure 2.

In our experiments, images from Pavia University dataset are randomly divided into 10% for training, and the remaining 90% are used for testing and evaluation. The model is trained for 100 epochs with batch size of 16. The optimization algorithm is Adam. The learning rate is set to 10^{-4}. The loss function is categorical cross-entropy. All models are implemented using Python, Keras framework that runs with TensorFlow back-end. The kappa coefficient (Kappa) and overall accuracy (OA) are adopted to evaluate the performance of the different networks.

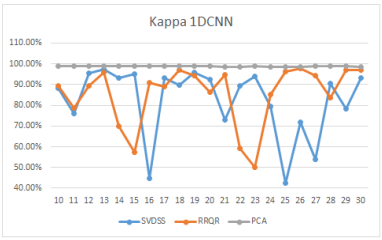

Fig. 3: Kappa results for 1D-CNN on Pavia University

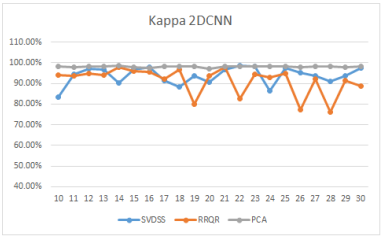

Fig. 4: Kappa results for 2D-CNN on Pavia University

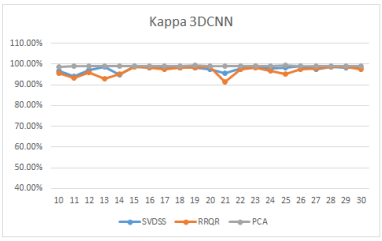

Fig. 5: Kappa results for 3D-CNN on Pavia University

4.2. Results

4.2.1. Dimensionality Reduction

In the experiments, CSS Algorithms discussed in section 2.2 are used to perform BSS as DR for the HSI. The number of bands selected for each method is varied from 10 to 30. Also, the results are compared to PCA, where the number of components varies from 10 to 30.

Fig. 3 to 5 show the resulting Kappa for each DR algorithm applied on the Pavia University scene as the number of bands or components is varied from 10 to 30. It is clear that Kappa varies by varying the subset of bands. PCA-based DR outperforms BSS techniques as it has the highest kappa for each model. Also, comparing Fig. 5 to Fig. 3 and Fig. 4 shows that 3D-CNN outperforms 2D-CNN and 1D-CNN, as 3D-CNN's kappa is always higher than 90%.

Table 1 shows the highest values of kappa for each DR method, along with the corresponding number of bands in case of SVDSS and RRQR, and components, in case of PCA. It shows by using 19 principal components, 3D-CNN classification model scores 99.32% Kappa. This is higher than 98.66% which was the score of Kappa after applying the 3D-CNN classification model to the full image.

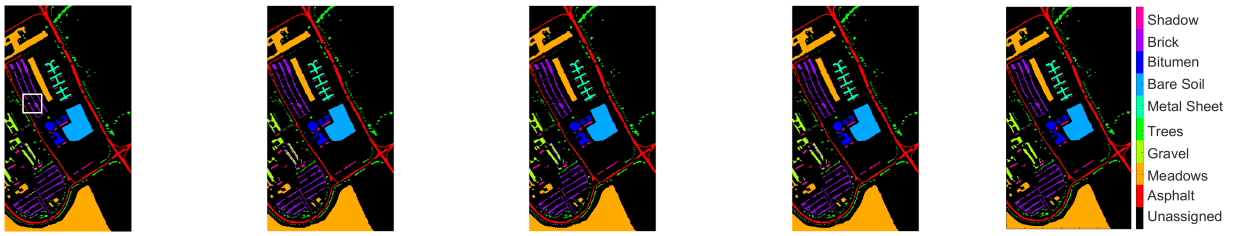

(a) 1D-CNN (b) 2D-CNN (c) 3D-CNN (d) HydraNet (Proposed) (e) Reference Class Map

Fig. 6: Classification results on Pavia University Dataset

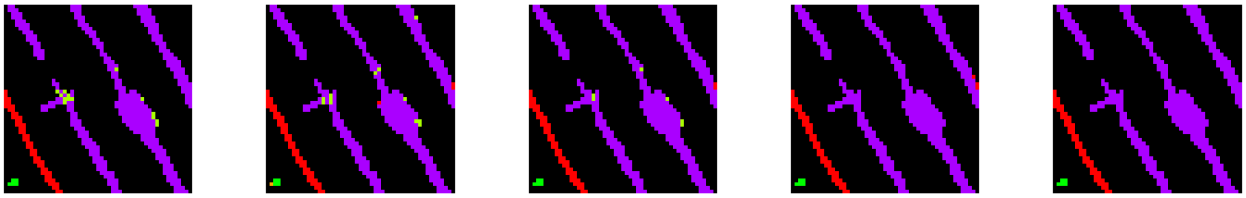

(a) 1D-CNN (b) 2D-CNN (c) 3D-CNN (d) HydraNet (Proposed) (e) Reference

Fig. 7: The area in the white box of Figure 6(a)

Table 1: Summary of Overall Accuracy (OA) and Kappa values over Pavia University using 3 DR approaches

		Model		
		1D-CNN	2D-CNN	3D-CNN
SVDSS	# Bands	13	22	26
	OA (%)	98.00	98.90	99.27
	Kappa (%)	97.37	98.54	99.03
RRQR	# Bands	28	21	28
	OA (%)	98.24	98.46	99.04
	Kappa (%)	97.67	97.96	98.72
PCA	# Bands	13	14	19
	OA (%)	**99.32**	**99.04**	**99.49**
	Kappa (%)	**98.90**	**98.55**	**99.32**
Full Image	OA (%)	91.72	93.56	98.99
	Kappa (%)	88.92	91.38	98.66

4.2.2. HydraNet Results

To demonstrate the performance of the proposed HydraNet architecture shown in Figure 1, classification results are compared to the constituents parts of the HydraNet; 1D-CNN, 2D-CNN, and 3D-CNN in addition to PMI-CNN [21] and MSR-3DCNN [22]. PCA is used as the pre-processing step for DR since it outperforms both RRQR and SVDSS. For qualitative evaluation, the classification maps obtained by four corresponding methods on Pavia University dataset are visually compared in Fig. 6. Figure 7 shows an enlarged area (marked by the white box in Figure 6(a)). It is observed that the result of our proposed method is closer to the reference map than those of all comparative methods.

The results in Table 2 show that our proposed HydraNet model obtains the best performance compared with the reference methods. In Comparison with 1D-CNN, 2D-CNN, 3D-CNN, PMI-CNN, and MSR-3DCNN the increase in Kappa is 0.77%, 1.12%, 0.35%, 0.73% and 0.49% ,respectively. The classification OA is 99.88% which is the highest among all other methods

Table 2: Classification performance of different methods for the Pavia dataset. Bold indicates the best result

Model	1D-CNN	2D-CNN	3D-CNN	PMI-CNN	MSR-3DCNN	HydraNet
Kappa (%)	98.90	98.55	99.32	98.94	99.18	**99.67**
OA (%)	99.32	98.91	99.49	99.19	99.38	**99.88**

5. CONCLUSION

In this paper, two BSS techniques were studied as a pre-processing step for HSI classification, namely SVDSS and RRQR, and compared to PCA. The latter, which showed the best performance, is integrated with the proposed HydraNet architecture to enhance HSI classification accuracy. The proposed model is trained and tested using Pavia University dataset. Evaluations of the proposed model in terms of visual quality, Kappa of 99.67%, and OA of 99.88% show that it outperforms 1D, 2D, 3D, PMI, and MSR-3D CNNs. In future, this work can be extended to include any combination of classification models rather than the three particular models adopted for this research.

6. REFERENCES

[1] S. Ji, X. Ma, W. Wang, L. Yu, J. Geng, and H. Wang, "Hyperspectral image classification by parameters prediction networks," in *IGARSS 2019-2019 IEEE International Geoscience and Remote Sensing Symposium*. IEEE, 2019, pp. 3309–3312.

[2] M. B. Stuart, A. J. S. McGonigle, and J. R. Willmott, "Hyperspectral imaging in environmental monitoring: a review of recent developments and technological advances in compact field deployable systems," *Sensors*, vol. 19, no. 14, pp. 3071, 2019.

[3] M. Shimoni, R. Haelterman, and C. Perneel, "Hypersectral imaging for military and security applications: Combining myriad processing and sensing techniques," *IEEE Geoscience and Remote Sensing Magazine*, vol. 7, no. 2, pp. 101–117, 2019.

[4] S. Mei, X. Li, X. Liu, H. Cai, and Q. Du, "Hyperspectral image classification using attention-based bidirectional long short-term memory network," *IEEE Transactions on Geoscience and Remote Sensing*, vol. 60, pp. 1–12, 2021.

[5] K. Mounika, K. Aravind, M. Yamini, P. Navyasri, S. Dash, and V. Suryanarayana, "Hyperspectral image classification using svm with pca," in *2021 6th International Conference on Signal Processing, Computing and Control (ISPCC)*. IEEE, 2021, pp. 470–475.

[6] Y. Q. Zhao, L. Zhang, and S. G. Kong, "Band-subset-based clustering and fusion for hyperspectral imagery classification," *IEEE Transactions on Geoscience and Remote Sensing*, vol. 49, no. 2, pp. 747–756, 2010.

[7] M. Velez-Reyes, D. M. Linares, and L. O. Jimenez-Rodriguez, "Two-stage band selection algorithm for hyperspectral imagery," in *Proceedings of SPIE*, 2002, vol. 4725, pp. 30–37.

[8] Z. Zhao, D. Hu, H. Wang, and X. Yu, "Center attention network for hyperspectral image classification," *IEEE Journal of Selected Topics in Applied Earth Observations and Remote Sensing*, vol. 14, pp. 3415–3425, 2021.

[9] W. Hu, Y. Huang, L. Wei, F. Zhang, and H. Li, "Deep convolutional neural networks for hyperspectral image classification," *Journal of Sensors*, vol. 2015, 2015.

[10] K. Makantasis, K. Karantzalos, A. Doulamis, and N. Doulamis, "Deep supervised learning for hyperspectral data classification through convolutional neural networks," in *2015 IEEE International Geoscience and Remote Sensing Symposium (IGARSS)*. IEEE, 2015, pp. 4959–4962.

[11] M. Kanthi, T. H. Sarma, and C. S. Bindu, "A 3d-deep cnn based feature extraction and hyperspectral image classification," in *2020 IEEE India Geoscience and Remote Sensing Symposium (InGARSS)*. IEEE, 2020, pp. 229–232.

[12] N. Shazeer, K. Fatahalian, W. R. Mark, and R. T. Mullapudi, "Hydranets: Specialized dynamic architectures for efficient inference," in *2018 IEEE/CVF Conference on Computer Vision and Pattern Recognition*, 2018, pp. 8080–8089.

[13] M. Q. Alkhatib and M. Velez-Reyes, "Using band subset selection for dimensionality reduction in superpixel segmentation of hyperspectral imagery," in *2020 IEEE International Conference on Image Processing (ICIP)*. IEEE, 2020, pp. 26–30.

[14] Y. Chen, H. Jiang, C. Li, X. Jia, and P. Ghamisi, "Deep feature extraction and classification of hyperspectral images based on convolutional neural networks," *IEEE Transactions on Geoscience and Remote Sensing*, vol. 54, no. 10, pp. 6232–6251, 2016.

[15] G. H. Golub and C. F. Van Loan, *Matrix Computations*, The Johns Hopkins University Press, 4 edition, 2013.

[16] M. Velez-Reyes and L. O. Jimenez, "Subset selection analysis for the reduction of hyperspectral imagery," in *Proceeding of the 1998 IEEE International Geoscience and Remote Sensing. Symposium Proceedings (IGARSS)*. IEEE, 1998, vol. 3, pp. 1577–1581.

[17] G. H. Golub, V. Klema, and G. W. Stewart, "Rank degeneracy and least squares problems," Tech. Rep., Stanford University Department of Compute Science, 1976.

[18] T. F. Chan and P. C. Hansen, "Some applications of the rank revealing QR factorization," *SIAM Journal on Scientific and Statistical Computing*, vol. 13, no. 3, pp. 727–741, 1992.

[19] T. F. Chan and P. C. Hansen, "Low-rank revealing QR factorizations," *Numerical Linear Algebra with Applications*, vol. 1, no. 1, pp. 33–44, 1994.

[20] J. Bai, B. Ding, Z. Xiao, L. Jiao, H. Chen, and A. C. Regan, "Hyperspectral image classification based on deep attention graph convolutional network," *IEEE Transactions on Geoscience and Remote Sensing*, vol. 60, pp. 1–16, 2021.

[21] Huan Zhong, Li Li, Jiansi Ren, Wei Wu, and Ruoxiang Wang, "Hyperspectral image classification via parallel multi-input mechanism-based convolutional neural network," *Multimedia Tools and Applications*, pp. 1–26, 2022.

[22] Hao Xu, Wei Yao, Li Cheng, and Bo Li, "Multiple spectral resolution 3d convolutional neural network for hyperspectral image classification," *Remote Sensing*, vol. 13, no. 7, pp. 1248, 2021.